Robotics and Autonomous Systems 79 (2016) 58–71

Contents lists available at ScienceDirect

Robotics and Autonomous Systems

journal homepage: www.elsevier.com/locate/robot

Level-ground walking for a bipedal robot with a torso via hip series elastic actuators and its gait bifurcation control

Ka Deng, Mingguo Zhao *, Wenli Xu

Department of Automation and Tsinghua National Laboratory for Information Science and Technology, Tsinghua University, 100084, Beijing, China

HIGHLIGHTS

- A level-ground walking method for a bipedal robot with a torso is proposed.
- Hip SEAs support the torso as well as complement energy via elastic potential energy.
- Our simple control scheme can lead to an efficient and natural stable period-1 gait.
- A variety of bifurcation gaits are observed, many of which never reported before.
- Bifurcation gait can be controlled to period-1 gait, which has better performance.

ARTICLE INFO

Article history:
Received 11 September 2015
Accepted 24 January 2016
Available online 10 February 2016

Keywords:
Level-ground walking
Bipedal robot with a torso
Series elastic actuator
Gait bifurcation
Ott–Grebogi–Yorke method

ABSTRACT

Recent studies have shown that a bipedal robot with a torso supported by springs on the hip can have a stable passive gait on a slope, while such a robot walking on level ground is a new challenge and has rarely been studied. This research adds actuators in series with the springs to form series elastic actuators on the hip and applies a state machine as controller to achieve stable walking on level ground. During walking, hip series elastic actuators support the torso from the legs as well as complement the energy to the system via elastic potential energy. The state machine uses the landing impact of the swing leg and the actuation durations as events to make the robot switch between successive active and passive walking processes. Because this simple scheme makes full use of the dynamics of the robot, it can lead to an efficient and natural gait. By means of numerical simulation, in addition to the stable period-1 gait, we found a variety of gait bifurcation phenomena, including the period-doubling bifurcation, the Neimark–Sacker bifurcation, the Neimark–Sacker-2 bifurcation, the period-X bifurcation, and the Neimark–Sacker-X bifurcation, among which many types have never been reported in previous studies. We also show that the unstable period-1 gait embedded in the bifurcation gait can be stabilized by applying the Ott–Grebogi–Yorke method. Not only can the gait bifurcation be suppressed, but also higher gait performance can be achieved.

1. Introduction

Since 'passive dynamic walking' was introduced by McGeer [1] in the late 1980s, the torso has been abolished in walking models. However, recently, a growing number of researchers have turned their attention to bipedal walking robots with torsos, which are more human-like. In addition, adding a torso to a robot has practical benefits, such as allowing more manipulations or interactions by installing arms or a head, and holding electronics or batteries in the trunk. Investigating more about walking with a torso may improve the application of the bipedal robot. In 2000, Chatterjee et al. [2] proposed a possible solution: adding a torso to the passive bipedal walking model via hip springs, but they did not realize it. In 2005, using this model, Gomes et al. [3] succeeded in realizing collision-less walking on level ground in simulation, however, such a gait with exaggerated unnatural movement was quite different from human gait and was also unstable, which made it lack practicability. In 2011, Chyou et al. [4] continued to work on this model. They presented stable passive gaits on a slope and showed that the stability and efficiency can be improved with a torso via springs. In 2012, the authors [5] found that two stable period-1 gaits can co-exist with certain model parameters. Farshimi et al. [6] also showed multiple routes to chaos in the passive gait of the simplest walking model with a torso added via hip springs. The above results demonstrate that hip springs can help in passively adding a

* Corresponding author.
E-mail address: mgzhao@mail.tsinghua.edu.cn (M. Zhao).

http://dx.doi.org/10.1016/j.robot.2016.01.013
0921-8890/

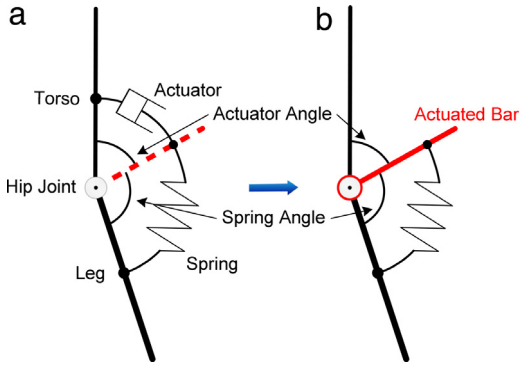

Fig. 1. Schematics of the hip series elastic actuator.

torso to a bipedal walking robot, and such a robot can realize stable passive walking on a slope. However, level-ground walking using this model is a new challenge and an important issue for its practical application, which has rarely been studied yet. If suitable actuations are added, the level-ground walking gait will be efficient and natural compared with those robots controlled by high-gain control, which motivates us to go ahead with the research. This study makes further use of the hip springs to achieve stable level-ground walking: specifically, it uses series elastic actuators as hip actuators and a state machine as a controller.

Using series elastic actuators for hip actuation is inspired by the human hip structure. There are natural elastic actuation structures in the human hip: the muscle–tendon unit, including the hip extensor—gluteus maximus; and the hip flexors—iliacus and psoas [7,8]. Both of these act on the hip joint antagonistically, stabilizing the torso and protracting and retracting legs during walking. In the muscle–tendon unit, the muscle acts as an actuator and the tendon can be modeled as a passive elastic element [8]. Because under most normal walking conditions, the tendon can be seen as a linear spring [9], and because the elasticity of the muscle fiber is insignificant compared with that of the tendon [10], the antagonistic muscle–tendon units at the hip can be imitated by an actuator in series with a linear spring, whose structure is similar to the MIT series elastic actuator introduced by Pratt et al. [11]. Various SEAs have been successfully applied in bipedal robots and prostheses [12–16], and they usually use a force/torque control mode. In this research, the springs are used as potential energy storage devices to replenish the system energy and realize level-ground walking. The actuator in the SEA deforms the spring to regulate its elastic potential energy.

The hip SEA in this study is shown as (a) in Fig. 1. It is mounted between the torso and the leg. The actuator is installed on the torso and its output is connected to one end of the spring. The other end of the spring is attached to the leg. The actuator can make a bi-directional movement, i.e., the spring can be compressed or stretched. To facilitate understanding in the later part of the manuscript, the output of the actuator, i.e., the actuator angle in Fig. 1, will be represented by the red actuated bar as shown in (b). The output torque is determined by the deformation of the spring, namely the difference between the spring angle in Fig. 1 and the equilibrium angle of the spring.

Many active control methods to realize level-ground walking in a bipedal robot with a torso exist, and act to control the torso posture [17–21], control the relative angle between the torso and the stance leg [22], or directly track a reference posture trajectory [23,24]. These methods rely on high-gain feedback control, which damages the passive dynamics of the robot, resulting in inefficient and unnatural gaits. Furthermore, these methods produce high demand on the model fidelity and the actuator performance, which make them difficult to execute successfully. Narukawa et al. [21] added a spring in parallel with the actuator on the hip that successfully reduced the torque cost of the actuator, but still left the disadvantages introduced by the real-time feedback control and the unnatural torso posture that leans noticeably forward during walking unsolved. La Hera et al. [24] devised a systematic trajectory planning procedure for realizing stable level-ground walking of a planar bipedal walker with a torso supported by springs, which is actuated in between the legs. The periodic motion was implemented by a complicated nonlinear exponentially orbitally stabilizing feedback controller with time-invariant gain, and the torso inclination during walking is significant and unnatural as well.

Hip SEA provides new and easier ways to achieve natural and efficient walking on level ground. During human walking, the muscles drive the leg only when appropriate, and most free leg swing is driven by gravity [25–27]. In previous studies of walking robot, it has been discovered that the actuation does not need to work throughout the walking process, and that efficient and natural motion can be generated by only applying actuation at a few key instants while the rest of the walking process remains passive. Pratt et al. [12,28], Wisse et al. [29,30], Raibert et al. [31–33] and the author's colleagues [34–36] have all verified this principle in their walking or hopping robots such that complicated motion can be implemented by a simple event-based state machine. Events, i.e., the switch condition of the state machine, can be triggered by the system state or the system clock, which can be very flexible in its selection. In this study, the events are chosen from those that can be easily obtained in the system, such as detecting the landing impact of the swing leg by a switch under the feet and timing the actuation duration via the system clock.

Considering the concrete approaches to realizing level-ground walking based on the passive dynamics of the bipedal robot, some previous researchers have introduced actuations and controls to replace the slope to supply energy to the system [29,30,37–41]. Such methods effectively use the dynamics of the robot, resulting in an efficient and natural gait. Because of the similarity between elastic potential energy and gravitational potential energy, springs in the SEAs can be used as a medium to store and control energy to achieve stable walking on level ground.

A bipedal walking robot is a typical hybrid nonlinear system. Since the bifurcation and chaos phenomena in passive dynamic walking models were first reported by Goswami et al. [42] in 1996, they have attracted the continuous attention of scientists in various fields. In 2014, Iqbal et al. [43] reviewed more than 100 papers on bifurcation and chaos in passive dynamic walking and its control issues. Among them, there are two results closely related to our study: Chyou et al. [4] discovered that period-doubling bifurcation gait appeared in the compass-like model with a torso supported by hip springs with increasing slope angle; and Farshimi et al. [6] found that there were various routes to chaos in the simplest walking model with a torso supported by hip springs, and the growth of the mass ratio of the torso to the hip would cause quasi-period bifurcation, namely Neimark–Sacker bifurcation. In our model, not only the torso and the springs, but the actuation and control via the hip SEAs are involved, therefore, we have more means to take advantage of the unique characteristics of this nonlinear system. The main advantage of the proposed actuated system is that its control parameters are time durations and angular position, which are easy to be controlled in practice.

As in a normal nonlinear dynamic system, there is an unstable period-1 gait embedded in the bifurcation gait. Comparing this with the bifurcation gait, the latter has more diverse walking patterns while the former has advantages in terms of energy efficiency and walking speed. Asano et al. [44,45] used a rimless wheel model to show that symmetric (period-1) gait had better energy efficiency. Harata et al. [46,47] also found that the period-1

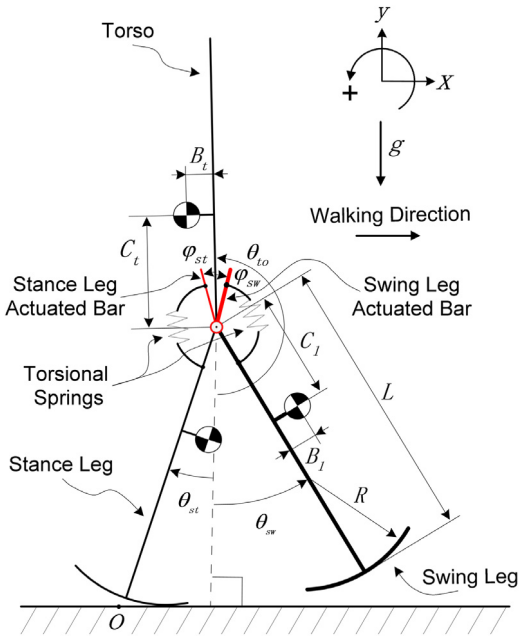

Fig. 2. Bipedal robot with a torso coupled with hip series elastic actuators.

gait had a higher speed. If the gait bifurcation can be suppressed by means of control, the unstable period-1 gait can be stabilized and the walking performance will be improved. In previous studies, the main approaches to control bifurcation or chaos in walking include the Ott–Grebogi–Yorke (OGY) method [48], the delayed feedback control (DFC) method [49] and artificial neural networks. Suzuki et al. [50] expanded the slope range of stable passive walking and achieved fast non-chaotic walking on a steep slope using the OGY method. Gritli et al. [51,52] used a linearization of the controlled Poincaré map around its fixed point to assist the design of the stabilizing control law based on the OGY method, and validated it on a compass-like walker and a torso-driven bipedal robot. Harata et al. [46,47] used the DFC method to stabilize a period-2 gait to a period-1 gait. Asano et al. [45] also used the DFC method, together with a quasi-constraint on the impact posture, to suppress the period-2 gait exhibited in virtual passive dynamic walking. Kurz et al. [53,54] exploited an artificial neural network to tune the hip actuation and successfully stabilize the chaotic gait. In this paper, bifurcation gaits, including some rare types, are suppressed to the embedded unstable period-1 gaits by applying the OGY method for better walking performances.

This paper is structured into five sections. In Section 2 the level-ground walking model is introduced. With a detailed model of the bipedal robot, the dynamics equations during walking are derived. Section 3 presents the effects of the control parameters on the gait via the simulation results, including period-1 gait and bifurcation gaits under different control parameters and their walking performance. In Section 4, the OGY method is applied to stabilize the bifurcation gait. In Section 5, conclusions are drawn and future work is discussed.

2. Level-ground walking model

2.1. Model

Based on previous research [5], straight legs with arc feet were chosen to mimic the bipedal structure. Then, a torso was added with hip series elastic actuators between the torso and legs. The model is shown in Fig. 2. This study concentrates on level-ground walking in the sagittal plane, hence the lateral movement is ignored.

In the model, the legs and the torso are all straight rigid bars articulated at the hip joint with no damping or friction. The mass of each part is concentrated at the center of mass (CoM), the position of which is described by the relative offset from the hip joint. The hip series elastic actuator is made up of an actuator in series with a torsional spring, which is placed between the leg and the actuated bar; the actuator is mounted on the torso. The actuated bar rotates around the hip to change the position of one end of the spring, thereby affecting the deformation of the spring as well as the motion of the robot.

Further details about the model:

- Coordinate system: As shown in Fig. 2, in each step, a two-dimensional Cartesian coordinate system is established with the origin at point 'O'. 'O' is the point where the center of the stance leg arc foot touches the ground when it rolls during one step, namely the contact point of the stance leg arc foot with the ground when the stance leg is standing upright. The x-axis is parallel to the ground and points in the walking direction of the robot. The y-axis is directed vertically upward.
- Arc foot: According to previous research results [1,55], the radius of the arc foot is set to be 0.3 times the leg length, and the mass is ignored.
- Series elastic actuator: The masses of the SEAs are merged into the mass of the torso. The springs are massless linear torsional springs.
- Mass distribution: To make the mass distribution of the robot close to that of a human, namely so that the CoM of the whole body is located around the hip, the mass of the torso is set to be the sum of the two legs and the CoM locations of the torso and legs are set to be symmetric with respect to the hip.

The posture of the robot can be described by the angle of the legs and the torso with respect to the vertical line to the ground, symbolized as θ_{st}, θ_{sw} and θ_{to} for the stance leg angle, the swing leg angle and the torso angle respectively. The positive directions of these three angles are defined as the counter-clockwise direction. The angles between the torso and the actuated bars for the stance leg and the swing leg respectively are defined as ϕ_{st} and ϕ_{sw}, whose positive direction is counter-clockwise as well, and whose zero positions coincide with the torso. So, the equilibrium position of the robot is $\theta_{st} = 0, \theta_{sw} = 0, \theta_{to} = \pi$ with $\phi_{st} = 0$ and $\phi_{sw} = 0$.

To make this research more universal, the parameters of the model are non-dimensionalized. The leg length, the foot radius and the CoM offsets are divided by the leg length. The masses of the legs and the torso are divided by the leg mass. The inertias are divided by the leg mass times the square of the leg length. Time parameters are divided by the arithmetic square root of the ratio of the real gravitational acceleration to the leg length, and the unit of non-dimensionalized time is denoted as $\tilde{s}$. The elastic coefficient of the torsional spring is divided by the production of the real gravitational acceleration, the leg length and the leg mass. Then, the gravitational acceleration of the model is non-dimensionalized to one.

The symbols and the default values of the non-dimensional parameters are listed in Table 1. These default values make reference to the human body structure (e.g., mass distribution), the previous study (e.g., foot radius in [1,55]), and the reasonable value that performs well in the simulation and takes into account the physical meaning (e.g., spring coefficient).

Some basic assumptions about locomotion:

- Contact with the ground: During walking, the foot of the stance leg is always in contact with the ground without sliding.
- Impact: When the swing leg lands on the ground, there will be an impact, which is assumed to be instantaneous and is

Table 1
Symbols and default values of robot parameters.

Parameter	Symbol	Default value
Leg length	L	1
Leg CoM normal offset	B_l	0
Radial offset	C_l	0.35
Torso CoM normal offset	B_t	0
Radial offset	C_t	0.35
Foot radius	R	0.3
Leg mass	m_l	1
Torso mass	m_t	2
Leg inertia	I_l	0.14
Torso inertia	I_t	0.28
Elastic coefficient of torsional spring in SEA	k	5
Equilibrium angle of torsional spring in SEA	ϕ_0	π
Gravitational acceleration	g	1

modeled as a perfect inelastic collision without any bounce or slipping. The impact makes the former swing leg to become the new stance leg, while the former stance leg leaves the ground to be the new swing leg. At the instant of impact, the momentum of the robot about the contact point of the foot of the swing leg with the ground is conserved, which leads to a discontinuous change in angular velocity with the posture unchanged. Thus, the potential energy will remain constant while the kinetic energy jumps immediately.

- Scuffing: As a straight-legged model is used, scuffing will occur when the swing leg passes by the stance leg. In the simulation, just like in other straight-legged robot research [56], scuffing will be ignored.

To facilitate the discussion later, some basic concepts and definitions are given here:

- Step: In this paper, a step refers to the process from the take-off of the swing leg from the ground to its landing. It starts with the previous impact and ends with the subsequent impact. The indicators, such as step frequency and step length, all refer to this definition of a step.
- Poincaré section and Poincaré map: In this paper, the Poincaré section is set to capture the state at the initial instant of each step. In locomotion research, to facilitate analysis, it is common to transform the continuous walking process into a Poincaré map, i.e., the map between the states of adjacent steps on the Poincaré sections.
- Initial state: It is the state of the robot at the beginning of one step, which is also the state just after the impact of last step.
- Period-1 gait: It, also called a single-period gait or symmetric gait, refers to a gait wherein any two adjacent steps are exactly the same, i.e., the states of the robot repeat themselves exactly from step to step.
- Period-X gait: It is a gait with an integer period X greater than 1. The motion repeats every X steps, and each adjacent step is distinct.
- Quasi-period gait: In quasi-period gait, no integer period can be found although the motion looks cyclical. The repetition of the movement is inaccurate, which makes the period non-integral.

2.2. Walking process

The actuation of the robot is implemented at the beginning of each step. The followings are some considerations for this arrangement. First, we want to imitate an important feature existing in human gait, i.e., the swing leg is boosted to swing forward at the beginning of one step, which is related to the pelvic rotation when a human walks [57]. Second, according to the common sense of walking gait, at the beginning of one step, the legs of the robot are spread apart, so the deformations of the springs are large, which enables the actuators to complement more

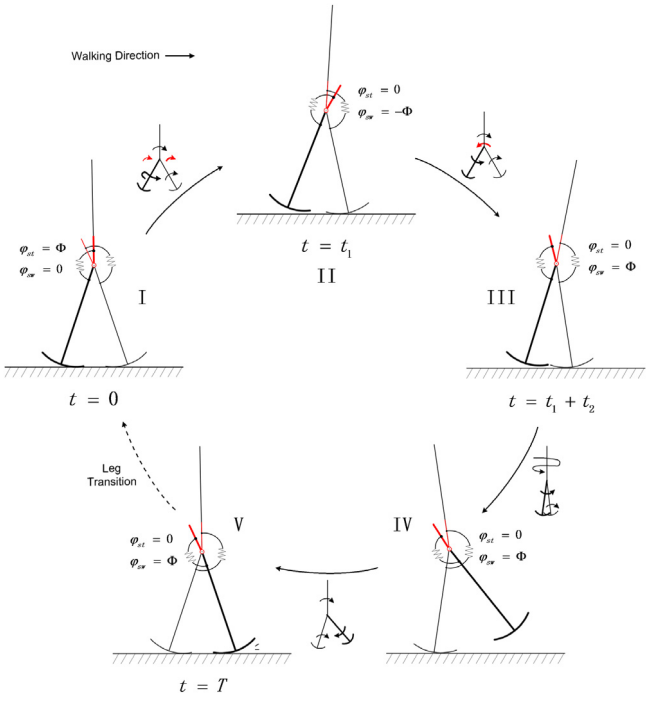

Fig. 3. The walking process of one step. Each big schematic numbered by Roman numerals represents an instant. The red arrows on the small schematics describe the swing directions of the actuated bars, and the black ones describe the swing directions of the torso and legs. (For interpretation of the references to color in this figure legend, the reader is referred to the web version of this article.)

energy with a certain actuator angle. In order to take advantage of this feature, the actuation is arranged at the beginning of the step.

In this walking model, there are five instants, as shown in Fig. 3, which separate the whole step into three stages and one instantaneous process: the first actuated stage (I–II), the second actuated stage (II–III), the unactuated stage (III–V), and the instantaneous impact at the heel strike (V). The three stages constitute the swing phase of one step.

The active actuation happens in the first two stages. There are three important parameters closely related to the actuation process: the durations of the first two stages, t_1 and t_2, and the maximum swing angle of the actuated bar, Φ.

The detailed actuation process is as follows. The swing movements of the actuated bars are shown in Fig. 4.

(1) The first actuated stage (I–II):
This stage begins at $t = 0$ and lasts t_1, so $t \in [0, t_1)$. In this stage, the actuated bar of the stance leg swings uniformly from $\varphi_{st} = \Phi$ to the zero position $\varphi_{st} = 0$; meanwhile, the actuated bar of the swing leg swings uniformly from the zero position $\varphi_{sw} = 0$ to $\varphi_{sw} = -\Phi$.

(2) The second actuated stage (II–III):
This stage starts just after the end of the previous stage and lasts for t_2, so $t \in [t_1, t_1 + t_2)$. In this stage, the actuated bar of the stance leg remains at the zero position and the actuated bar of the swing leg sways back from $\varphi_{sw} = -\Phi$ to $\varphi_{sw} = \Phi$.

(3) The unactuated stage (III–V):
This stage starts at $t = t_1 + t_2$, and its termination time cannot be known in advance and is determined by the heel strike. In Fig. 3, the landing time of the swing leg is assumed to be $t = T$, which is also the duration of the whole step. There is no actuation, so this stage is termed the 'unactuated stage'. The actuated bars stop in the position that they were in at the beginning of the current stage, i.e., $\varphi_{st} = 0$ and $\varphi_{sw} = \Phi$. The SEAs on the hip can be regarded as passive springs. IV is the instant when the swing leg swings to the highest position. After

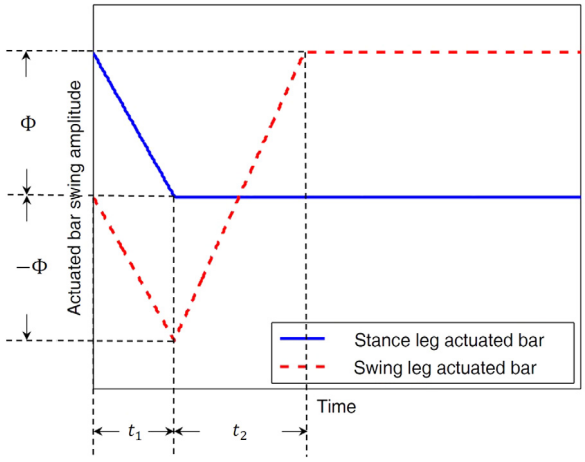

Fig. 4. The swing movements of the actuated bars during one step.

this instant, the swing leg begins to retract and the sign of its angular velocity changes.

(4) The heel strike (V):
The impact at the heel strike completes instantaneously without any actuation, so the robot is passive at this instant. It is obvious that, V in the current step and I in the next step are the same instant. The beginning of one step is triggered by the last heel strike, and the time will be reset to $t = 0$ immediately after the heel strike.

2.3. Dynamic equations

In the following, the dynamics of the robot in one step are derived by parts. By combining them together, the Poincaré map, known as the stride function, can be obtained. These dynamic equations are the bases of the numerical simulation.

The walking process can be divided into the three stages of the swing phase and an instantaneous impact at the heel strike. The dynamics of the swing phase can be presented in the form of differential equations, and the dynamics of the impact can be presented in the form of algebraic equations. The dynamics of the three stages are different in their elastic terms, thereby in the following, the general dynamics of the swing phase will be established first, and then the differences between the three stages will be presented. After that, the dynamics of the impact will be given.

2.3.1. Dynamics of the swing phase

(1) *General dynamics*. First, in the Cartesian coordinate system defined in Section 2.1, let us denote the CoM coordinates of both legs and the torso as $\boldsymbol{X}_{st} = [x_{st}, y_{st}]^T$, $\boldsymbol{X}_{sw} = [x_{sw}, y_{sw}]^T$ and $\boldsymbol{X}_{to} = [x_{to}, y_{to}]^T$. Then, the vector $\boldsymbol{x}$ is defined as $\boldsymbol{x} := [x_{st}, y_{st}, \theta_{st}, x_{sw}, y_{sw}, \theta_{sw}, x_{to}, y_{to}, \theta_{to}]^T$, containing the CoM positions and the angles of the legs and the torso.

Applying Newton's second law, the dynamics of the swing phase can be expressed as follows:

$$\boldsymbol{M}\ddot{\boldsymbol{x}} = \boldsymbol{F_g} + \boldsymbol{F_e} + \boldsymbol{F_c} \tag{1}$$

where $\boldsymbol{M} = diag(m_l, m_l, I_l, m_l, m_l, I_l, m_t, m_t, I_t)$ is the mass and inertia matrix, $\boldsymbol{F_g} = \boldsymbol{M}g[0, -1, 0, 0, -1, 0, 0, -1, 0]^T$ is the gravity related force/torque vector, $\boldsymbol{F_e} = [0, 0, \tau_{st}, 0, 0, \tau_{sw}, 0, 0, \tau_{to}]^T$ is the elasticity related force/torque vector and the details about the three torque components τ_{st}, τ_{sw} and τ_{to} will be explained later, and $\boldsymbol{F_c}$ is the internal constraint force/torque vector.

As there is redundancy in $\boldsymbol{x}$, the generalized coordinate $\boldsymbol{q} := [\theta_{st}, \theta_{sw}, \theta_{to}]^T$ is introduced to further reduce the dimensionality and facilitate the analysis. The vector $\boldsymbol{x}$ can be expressed as $\boldsymbol{x} = \boldsymbol{x}(\boldsymbol{q})$, and the three CoM coordinates are shown as follows:

$$\begin{cases} \boldsymbol{X}_{st} = \boldsymbol{Rot}\,(\theta_{st}) \cdot [B_l, C_l]^T + \boldsymbol{X}_{hip} \\ \boldsymbol{X}_{sw} = \boldsymbol{Rot}\,(\theta_{sw}) \cdot [B_l, C_l]^T + \boldsymbol{X}_{hip} \\ \boldsymbol{X}_{to} = \boldsymbol{Rot}\,(\theta_{to}) \cdot [B_t, C_t]^T + \boldsymbol{X}_{hip} \end{cases} \tag{2}$$

where $\boldsymbol{Rot}$ is the rotation matrix, defined as $\boldsymbol{Rot}\,(\cdot) := \begin{bmatrix} \cos(\cdot) & -\sin(\cdot) \\ \sin(\cdot) & \cos(\cdot) \end{bmatrix}$, and $\boldsymbol{X}_{hip}$ is the coordinate of the hip joint, which is expressed as $\boldsymbol{X}_{hip} = [-(R\theta_{st} + (L - R)\sin(\theta_{st})), R + (L - R)\cos(\theta_{st})]^T$.

Derived from $\boldsymbol{x} = \boldsymbol{x}(\boldsymbol{q})$,

$$\ddot{\boldsymbol{x}} = \frac{\partial \boldsymbol{x}}{\partial \boldsymbol{q}}\ddot{\boldsymbol{q}} + \frac{d}{dt}\left(\frac{\partial \boldsymbol{x}}{\partial \boldsymbol{q}}\right)\dot{\boldsymbol{q}} \tag{3}$$

where $\frac{\partial \boldsymbol{x}}{\partial \boldsymbol{q}}$ is the Jacobian matrix of $\boldsymbol{x}$ about $\boldsymbol{q}$, denoted by $\boldsymbol{J}$. So Eq. (3) can be rewritten as:

$$\ddot{\boldsymbol{x}} = \boldsymbol{J}\ddot{\boldsymbol{q}} + \dot{\boldsymbol{J}}\dot{\boldsymbol{q}}. \tag{4}$$

Substituting Eq. (4) into Eq. (1),

$$\boldsymbol{M}\boldsymbol{J}\ddot{\boldsymbol{q}} + \boldsymbol{M}\dot{\boldsymbol{J}}\dot{\boldsymbol{q}} = \boldsymbol{F_g} + \boldsymbol{F_e} + \boldsymbol{F_c}. \tag{5}$$

According to the principle of virtual work, $\boldsymbol{J}^T \cdot \boldsymbol{F_c} = 0$. So, by eliminating $\boldsymbol{F_c}$ in Eq. (5), the general dynamics of the swing phase is

$$\boldsymbol{J}^T\boldsymbol{M} \cdot \left(\boldsymbol{J}\ddot{\boldsymbol{q}} + \dot{\boldsymbol{J}}\dot{\boldsymbol{q}}\right) = \boldsymbol{J}^T \cdot \left(\boldsymbol{F_g} + \boldsymbol{F_e}\right). \tag{6}$$

In all three stages, the gravity term $\boldsymbol{F_g}$ is the same, and different elastic term $\boldsymbol{F_e}$ will be presented in the following. Specifically, the torques acting respectively on the stance leg, the swing leg and the torso by the hip series elastic actuators, τ_{st}, τ_{sw} and τ_{to}, are different in these stages.

(2) *The first actuated stage*. In this stage, both actuated bars swing forward. The torques, τ_{st}, τ_{sw} and τ_{to}, are :

$$\begin{cases} \tau_{st} = k\cdot\left(\theta_{to} - \theta_{st} - \phi_0 + \Phi\cdot\left(1 - \dfrac{t}{t_1}\right)\right) \\ \tau_{sw} = k\cdot\left(\theta_{to} - \theta_{sw} - \phi_0 - \Phi\dfrac{t}{t_1}\right) \\ \tau_{to} = k\cdot\left(-2\theta_{to} + \theta_{st} + \theta_{sw} + 2\phi_0 \right. \\ \qquad \left. - \Phi\cdot\left(1 - \dfrac{2t}{t_1}\right)\right). \end{cases} \quad 0 \le t < t_1 \tag{7}$$

Substituting the elastic term $\boldsymbol{F_e}$ with torques in Eq. (7) into Eq. (6) will produce the dynamics of this stage.

(3) *The second actuated stage*. In this stage, the actuated bar of the stance leg stays at the zero position, i.e., coincides with the torso, and the actuated bar of the swing leg sways backward. The torques τ_{st}, τ_{sw} and τ_{to} can be expressed as

$$\begin{cases} \tau_{st} = k\cdot(\theta_{to} - \theta_{st} - \phi_0) \\ \tau_{sw} = k\cdot(\theta_{to} - \theta_{sw} - \phi_0 \\ \qquad -\Phi\cdot\left(1 - \dfrac{2\,(t - t_1)}{t_2}\right)\right) \\ \tau_{to} = k\cdot\left(-2\theta_{to} + \theta_{st} + \theta_{sw} + 2\phi_0 \right. \\ \qquad \left. + \Phi\cdot\left(1 - \dfrac{2\,(t - t_1)}{t_2}\right)\right). \end{cases} \quad t_1 \le t < t_1 + t_2 \tag{8}$$

Substituting $\boldsymbol{F_e}$ with torques in Eq. (8) into Eq. (6) will produce the dynamics of this stage.

(4) *The unactuated stage*. When $t \ge t_1 + t_2$, both actuated bars are fixed at the position where they were at $t = t_1 + t_2$, so there is no

active actuation and the output torque is completely determined by the posture of the robot.

$$\begin{cases} \tau_{st} = k \cdot (\theta_{to} - \theta_{st} - \phi_0) \\ \tau_{sw} = k \cdot (\theta_{to} - \theta_{sw} - \phi_0 + \Phi) \\ \tau_{to} = k \cdot (-2\theta_{to} + \theta_{st} + \theta_{sw} + 2\phi_0 - \Phi)\,. \end{cases} \quad t \geq t_1 + t_2 \tag{9}$$

Substituting $\boldsymbol{F_e}$ with torques in Eq. (9) into Eq. (6) will produce the dynamics of this stage. Until the swing leg lands on the ground, the robot is dominated by such dynamics.

2.3.2. Dynamics of the impact

(1) *Impact equation*. The impact does not affect the posture of the robot, but exchanges the roles of two legs. There will be a sudden jump in the kinetic energy, and the angular velocity of each part of the robot will be changed by the impact.

Based on the momentum theorem,

$$\boldsymbol{M}\dot{\boldsymbol{x}}^{+} = \boldsymbol{M}\dot{\boldsymbol{x}}^{-} + \boldsymbol{\rho} \tag{10}$$

where the subscripts '+' and '−' stand for the instant just after and before the impact, and $\boldsymbol{\rho}$ is the variation in momentum.

Transforming Eq. (10) into generalized coordinates,

$$\boldsymbol{M}\boldsymbol{J}^{+}\dot{\boldsymbol{q}}^{+} = \boldsymbol{M}\boldsymbol{J}^{-}\dot{\boldsymbol{q}}^{-} + \boldsymbol{\rho}. \tag{11}$$

It should be noted that in the calculation of $\boldsymbol{J}^{+}$, the origin has already changed to the origin of the next step. $\boldsymbol{J}^{-}$ has the same form as $\boldsymbol{J}$ in the swing phase.

According to the principle of virtual work, $\boldsymbol{J}^{+T} \cdot \boldsymbol{\rho} = 0$. The relationship between the angular velocity before and after the impact is presented below:

$$\boldsymbol{J}^{+T}\boldsymbol{M}\boldsymbol{J}^{+}\dot{\boldsymbol{q}}^{+} = \boldsymbol{J}^{+T}\boldsymbol{M}\boldsymbol{J}^{-}\dot{\boldsymbol{q}}^{-}. \tag{12}$$

Summarizing the above, the state in generalized coordinates just after the impact is

$$\begin{cases} \boldsymbol{q}^{+} = \boldsymbol{q}^{-} \\ \dot{\boldsymbol{q}}^{+} = \left(\boldsymbol{J}^{+T}\boldsymbol{M}\boldsymbol{J}^{+}\right)^{-1}\boldsymbol{J}^{+T}\boldsymbol{M}\boldsymbol{J}^{-}\dot{\boldsymbol{q}}^{-}. \end{cases} \tag{13}$$

Considering the role switch happening at the impact, the transition of the impact can be expressed as

$$\begin{bmatrix} \boldsymbol{q}^{new} \\ \dot{\boldsymbol{q}}^{new} \end{bmatrix} = \begin{bmatrix} \boldsymbol{H}\boldsymbol{q}^{+} \\ \boldsymbol{H}\dot{\boldsymbol{q}}^{+} \end{bmatrix} \tag{14}$$

where $\boldsymbol{H} = \begin{pmatrix} 0 & 1 & 0 \\ 1 & 0 & 0 \\ 0 & 0 & 1 \end{pmatrix}$.

(2) *Impact condition*. In the simulation, the impact condition is used to detect the instant when the swing leg lands on the ground. It is also the termination condition of the unactuated stage and the swing phase. When the swing foot is just about to land, there are some characteristic features: the swing leg is in front of the stance leg; the angle between the two legs is bisected by the vertical line according to the geometrical relationship; and the swing leg is falling to the ground from above, not passing through the floor from the bottom up. Mathematizing the above features, the impact condition can be expressed as

$$\begin{cases} \theta_{st} = -\theta_{sw} \\ \theta_{st} < \theta_{sw} \\ \dot{\theta}_{st} + \dot{\theta}_{sw} < 0. \end{cases} \tag{15}$$

2.3.3. Poincaré map

Eqs. (6), (13) and (14) and condition (15) represent the different parts of the dynamics of this robot in one step. By combining them together, one step can be described by the Poincaré map, denoted as $\boldsymbol{F}$:

$$\boldsymbol{s}_{n+1} = \boldsymbol{F}(\boldsymbol{s}_n) \tag{16}$$

where $\boldsymbol{s}_n := [\boldsymbol{q}_n, \dot{\boldsymbol{q}}_n]^T$ is the initial state of the nth step, i.e., the state on the Poincaré section.

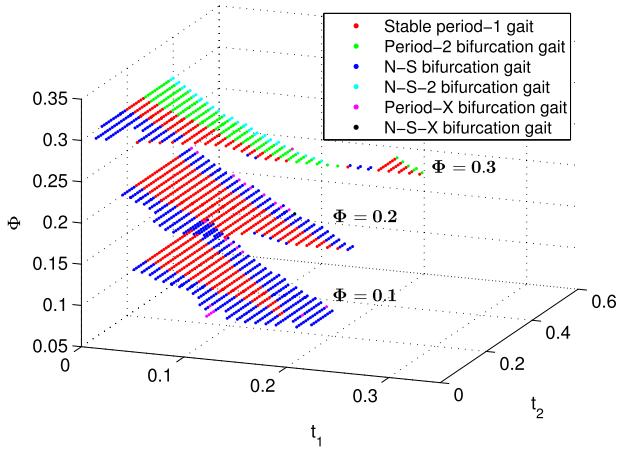

Fig. 5. The gait type distribution when $\Phi = 0.1$, 0.2 and 0.3. Each point represents a set of control parameters, and its color stands for the type of gait. The black dot is very rare, and the only case in the figure is located on the upper edge of the $\Phi = 0.2$ region. (For interpretation of the references to color in this figure legend, the reader is referred to the web version of this article.)

3. Effect of control parameters on gait

In this walking model, almost all the parameters, including t_1, t_2, Φ, k, B and C (CoM offsets), have significant effects on walking gait. Among them, t_1, t_2 and Φ are selected to be the control parameters, because they are easy to be controlled by timing and controlling motor angle in practice, while others are not. For instance, varying k needs a variable stiffness actuator, which is hard to realize nowadays in a real application. In this section, the influences of the control parameters on walking are revealed.

3.1. Various types of gaits

In this walking model, the control parameters will determine the type of gait. With different control parameters, there will be various types of gaits, including the stable period-1 gait and many bifurcation gaits. These bifurcation gaits are the period-doubling (period-2) bifurcation gait, the Neimark–Sacker (N–S) bifurcation gait, the Neimark–Sacker-2 (N–S-2) bifurcation gait, the period-X bifurcation gait and the Neimark–Sacker-X (N–S-X) bifurcation gait. The various walking patterns exhibit the diversity of the gaits.

Fig. 5 gives an example of gait distribution in control parameter space via numerical simulation. All the types of gait mentioned above are exhibited in the example.

The general principles of gait evolution are that the growth of Φ is the key to the period-doubling bifurcation, and the variations of t_1 and t_2 will give rise to N–S bifurcation. On the edge of some period-doubling and N–S regions, combinatorial types like N–S-2 or N–S-X bifurcation will occur. N–S-2 bifurcation always appears when Φ is between 0.2 and 0.3 while t_1 and t_2 are large. When Φ is too small, the period-doubling bifurcation will not happen, and when Φ is too large, the robot will end up with falling before its gait evolves into the N–S bifurcation. Furthermore, small t_1 and t_2 will only evoke N–S bifurcation, not N–S-2 bifurcation. N–S-2 bifurcation has multiple evolution routes, for instance, when $t_1 = 0.1$ and $\Phi = 0.3$, with increasing t_2, the gait will first evolve into

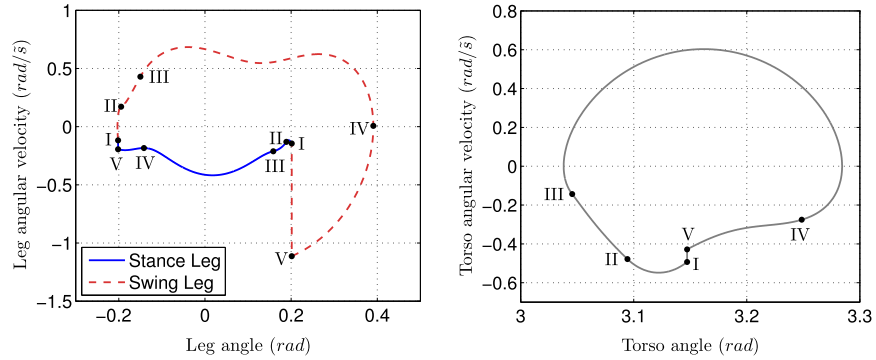

(a) Phase trajectory of legs. (b) Phase trajectory of torso.

Fig. 6. Phase diagrams of stable period-1 limit cycle ($t_1 = 0.1$, $t_2 = 0.17$, and $\Phi = 0.1$). The Roman numerals indicate the instants in Fig. 3.

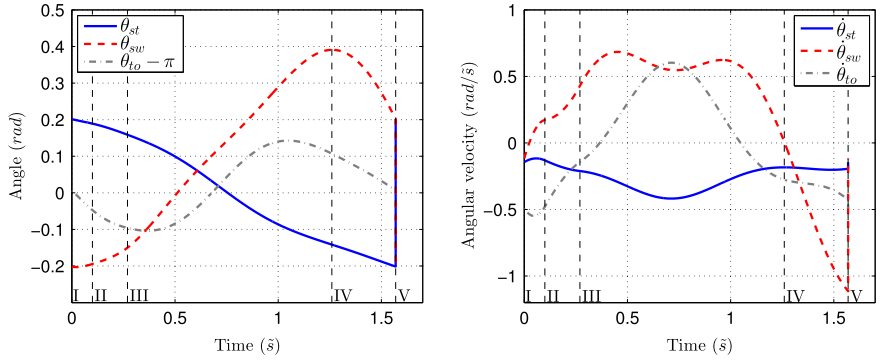

(a) Angle trajectories in one step. (b) Angular velocity trajectories in one step.

Fig. 7. The state trajectories in one step of the stable period-1 gait with respect to time. The whole duration of one step is segmented by the instants marked by black dashed lines with Roman numerals. (For interpretation of the references to color in this figure legend, the reader is referred to the web version of this article.)

the period-2 bifurcation gait from the stable period-1 gait, and then into the N–S-2 bifurcation gait; however, when $t_1 = 0.1$ and $\Phi = 0.25$, again, with increasing t_2, the route from the stable period-1 gait to the N–S-2 bifurcation gait becomes the N–S bifurcation gait. On the edge of period-doubling, N–S and N–S-2 regions, sometimes the quasi-period gait will become the integer-period gait, i.e., the period-X bifurcation occurs. Its evolution routes are various as well, but in general it occurs occasionally. N–S-X bifurcation is rarer, and its regularity in evolution is not obvious. However, all discovered N–S-X cases lie on the edge of the available control parameter region.

In the following, these types of gait will be exhibited and analyzed respectively by examples selected from Fig. 5.

3.1.1. Stable period-1 gait

An example of the stable period-1 gait, whose fixed point of the Poincaré map is $\boldsymbol{s}^* = [\boldsymbol{q}^{*T}, \dot{\boldsymbol{q}}^{*T}]^T = [0.2015, -0.2015, 3.1472, -0.1443, -0.1174, -0.4931]^T$, can be found when the control parameters are chosen as $t_1 = 0.1$, $t_2 = 0.17$, and $\Phi = 0.1$. Using this fixed point as the initial state, the states of the robot will form a stable limit cycle in phase space, as shown in Fig. 6.

During one step, the states of the robot vary with time as presented in Fig. 7. The stance leg swings forward monotonically. The swing leg first slightly sways backward when leaving the ground, and then swings to the front until it reaches the highest point, after which the swing leg retracts until it lands on the ground. The torso swings forward and then backward and finally forward to the original position. After the impact, the states are duplicated to the initial states. The torso wobbles around the upright position with a small amplitude less than 10 degrees during one step, as shown in the stick diagram in Fig. 8.

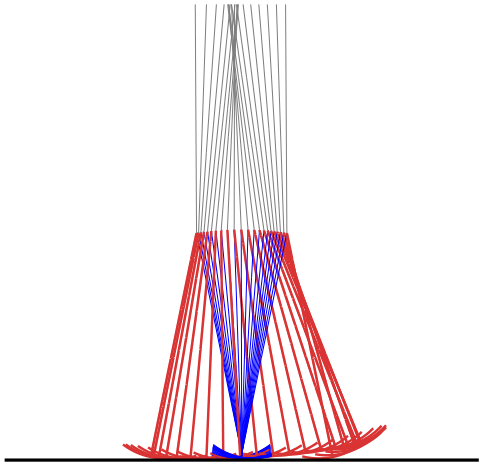

Fig. 8. Stick diagram of the robot during one step of the stable period-1 gait. The walking direction is from left to right. The colors of the torso and legs are consistent with Figs. 6 and 7: blue for stance leg, red for swing leg and gray for torso. (For interpretation of the references to color in this figure legend, the reader is referred to the web version of this article.)

Fig. 9 shows the energy transformation in one step. In the two actuated stages, I–III in Fig. 9, the mechanical energy of the robot increases, mainly contributed by the elastic potential energy. There is a little decline at the beginning, because in the first actuated stage, the energy stored in the spring between the swing leg and the torso is decreased. At the same time, the energy is supplemented to the system via the stance leg SEA. Overall, the total amount of mechanical energy is increased at the end of the first actuated stage. After III, the mechanical energy keeps

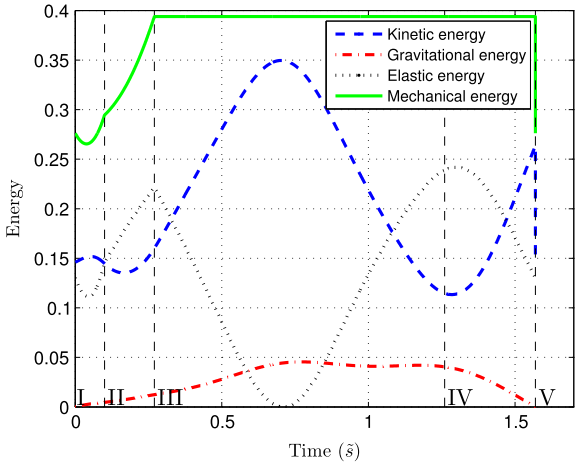

Fig. 9. Energy variation during one step. The energy has been non-dimensionalized. The actuation only takes place in I–III.

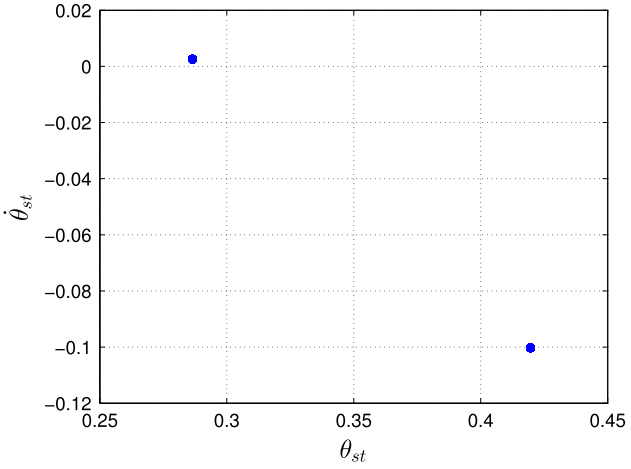

Fig. 10. The projection of the Poincaré section of the period-2 bifurcation gait ($t_1 = 0.1, t_2 = 0.14$, and $\Phi = 0.3$) on the $\theta_{st} - \dot{\theta}_{st}$ plane.

constant until the impact. The actuation completes within the first 0.27 $\tilde{s}$, which is about one sixth of the whole duration of the step. Therefore, most of the process is passive, which makes the gait energy efficient and natural. Just before the end of the step, the energy supplemented by the SEAs is all transformed into the kinetic energy. The energy loss caused by the impact equals to the supplementary energy, so the robot can keep on walking in a periodic pattern.

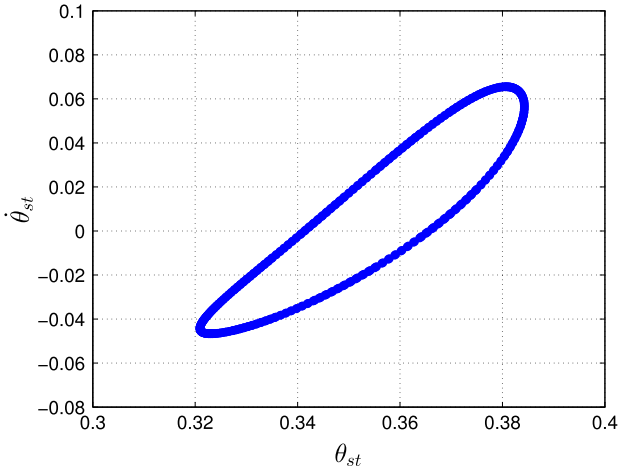

Fig. 12. The projection of the Poincaré section of the Neimark–Sacker bifurcation gait ($t_1 = 0.1, t_2 = 0.25$, and $\Phi = 0.2$) on the $\theta_{st} - \dot{\theta}_{st}$ plane.

3.1.2. Period-doubling (period-2) bifurcation gait

An example of period-doubling bifurcation gait can be observed when the control parameters are set as $t_1 = 0.1$, $t_2 = 0.14$, and $\Phi = 0.3$. There are two points on the Poincaré section, and they jump between each other in adjoining steps. Fig. 10 is the projection of the Poincaré section of the period-2 bifurcation gait on the $\theta_{st} - \dot{\theta}_{st}$ plane. At the critical bifurcation point, the maximum eigenvalue of the Jacobian matrix at the fixed point traverses the unit cycle at the point $(-1, 0)$ with the variation of the parameter, as shown in Fig. 11. The period-1 fixed point loses its stability and evolves into the period-2 pattern. In period-doubling bifurcation, except for the period-2 gait, bifurcation gait with higher 2^n periods is not observed. With the continuous variation of the parameters after period-2 bifurcation, the robot will fall or evolve into another kind of bifurcation.

3.1.3. Neimark–Sacker bifurcation gait

An example of the Neimark–Sacker bifurcation will occur when the control parameters are set as $t_1 = 0.1, t_2 = 0.25$, and $\Phi = 0.2$. The states on the Poincaré section are located on a closed invariant loop curve, which is the intersection of a torus in the phase space with the Poincaré section. Fig. 12 is the projection of the Poincaré section of the N–S bifurcation gait on the $\theta_{st} - \dot{\theta}_{st}$ plane. The way the fixed point changes stability is totally different from that of the period-doubling bifurcation. At the critical bifurcation point, the maximum eigenvalues of the Jacobian matrix at the fixed point traverse the unit cycle via a pair of complex numbers with unit modulus, $e^{\pm i\theta}$, $0 < \theta < \pi$, with the variation of the parameter, as shown in Fig. 13.

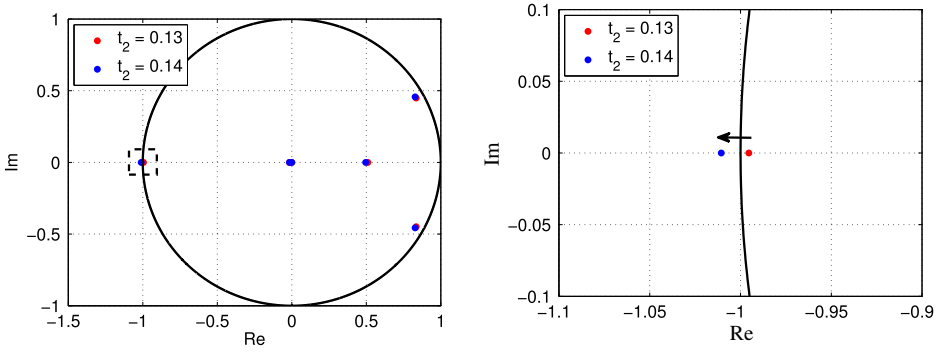

(a) All eigenvalues. (b) Local zoom of dashed rectangle in (a).

Fig. 11. Variation of eigenvalues of the Jacobian matrix at the fixed point when period-2 bifurcation occurs.

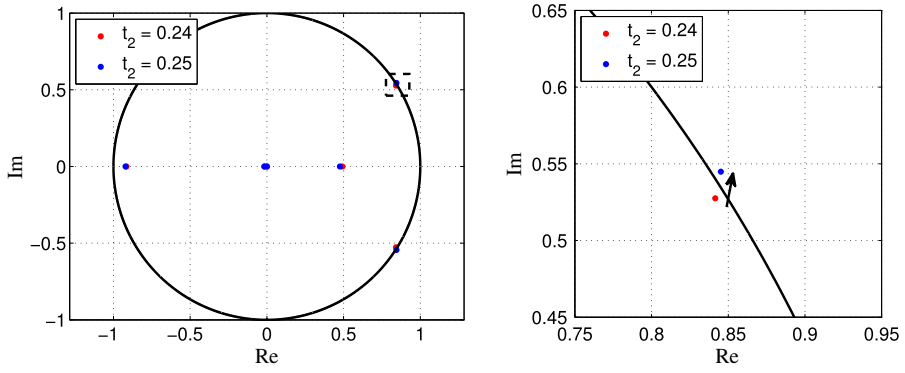

(a) All eigenvalues. (b) Local zoom of dashed rectangle in (a).

Fig. 13. Variation of eigenvalues of the Jacobian matrix at the fixed point when Neimark–Sacker bifurcation occurs.

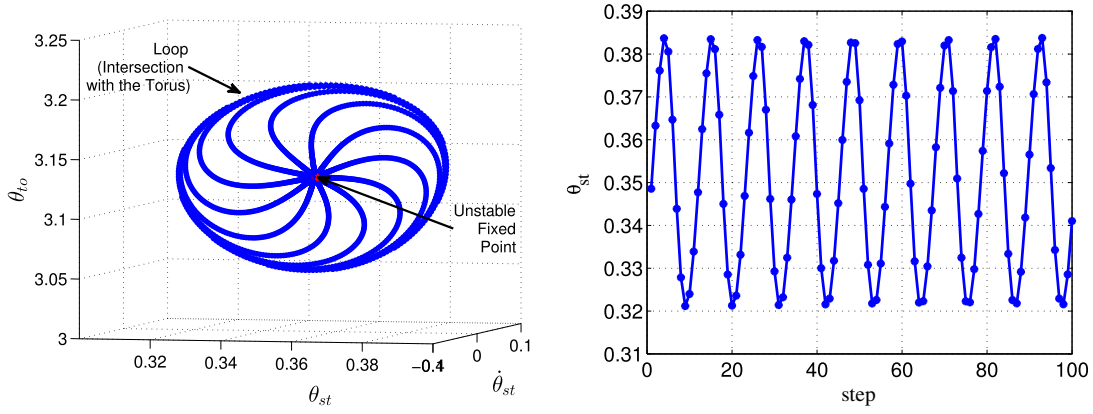

(a) Divergent process of N–S bifurcation. (b) Stance leg angle of 100 steps on the loop.

Fig. 14. Divergent process and quasi-period characteristic of the Neimark–Sacker bifurcation gait.

Fig. 14(a) presents the divergent process from the unstable period-1 fixed point to the loop (the intersection with the torus) on the Poincaré section projected to the $\theta_{st} - \dot{\theta}_{st} - \theta_{to}$ subspace. After the divergence completes, the approximate period is about 11 steps, i.e., a turn is taken around the loop every 11 steps but imprecisely. Fig. 14(b) displays the stance leg angle at the impact of 100 steps, which shows the quasi-period characteristic.

3.1.4. Neimark–Sacker-2 bifurcation gait

An example of the Neimark–Sacker-2 bifurcation gait will appear when the control parameters are set as $t_1 = 0.15$, $t_2 = 0.13$, and $\Phi = 0.3$. After bifurcation, a complicated torus is formed in the phase space that has two loops on the intersection with the Poincaré section, and the states jump between the loops step by step like in the period-doubling bifurcation. Fig. 15 is the projection of the Poincaré section after bifurcation.

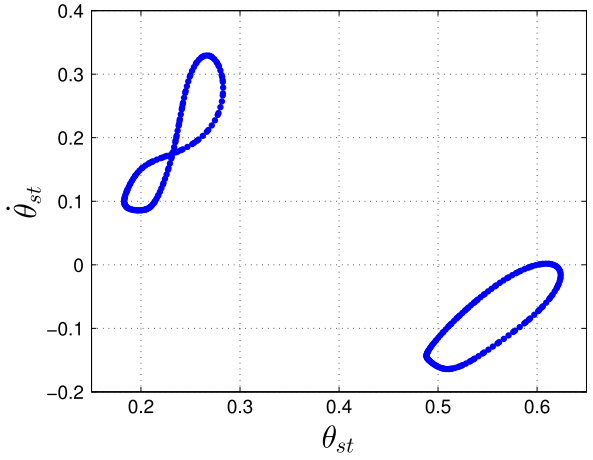

Fig. 15. The projection of the Poincaré section of the Neimark–Sacker-2 bifurcation gait ($t_1 = 0.15$, $t_2 = 0.13$, and $\Phi = 0.3$) on the $\theta_{st} - \dot{\theta}_{st}$ plane.

3.1.5. Period-X bifurcation gait

An example of the period-X bifurcation gait, which has an integer period just like Fig. 16(a), can be observed when the control parameters are set as $t_1 = 0.1$, $t_2 = 0.29$, and $\Phi = 0.2$, The states on the Poincaré section still look like a loop, but the integer period characteristic distinctly sets it apart from the N–S bifurcation. If this bifurcation happens on the edge of the N–S-2 bifurcation region, like $t_1 = 0.19$, $t_2 = 0.07$ and $\Phi = 0.3$, the states on the Poincaré section will be like two loops as shown in Fig. 16(b), and jump between them step by step. In this case, period-X bifurcation does not include period-doubling bifurcation. Although both of them have integer periods, they can be easily distinguished by their evolution regularity and distribution in parameter space; what is more, the periods in the period-X bifurcation cases are all apparently larger than 2.

3.1.6. Neimark–Sacker-X bifurcation gait

An example of the Neimark–Sacker-X bifurcation gait can be observed when the control parameters are set as $t_1 = 0.17$, $t_2 =$

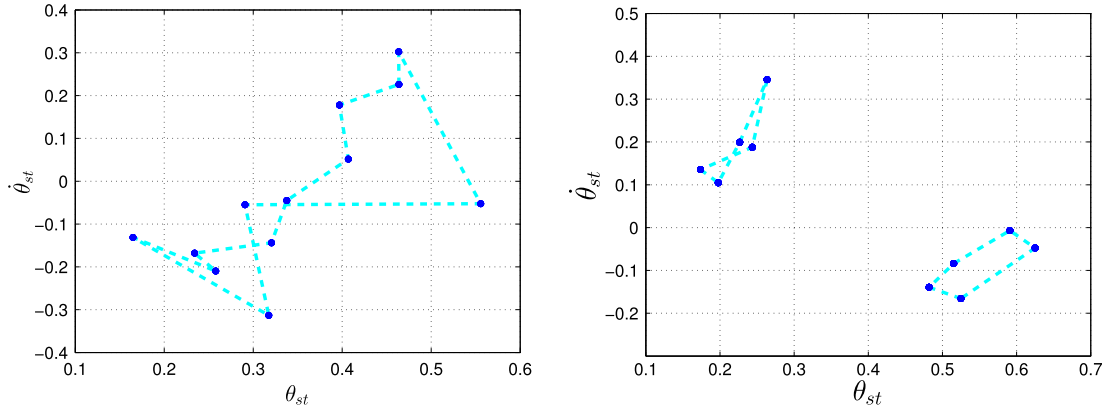

(a) Single loop case.

(b) Double loops case.

Fig. 16. The projection of the Poincaré section of the period-X bifurcation gait ($t_1 = 0.1$, $t_2 = 0.29$, and $\Phi = 0.2$) on the $\theta_{st} - \dot{\theta}_{st}$ plane. The deep blue point is the state point at each step and the light blue dashed lines are virtual connections. (For interpretation of the references to color in this figure legend, the reader is referred to the web version of this article.)

0.17, and $\Phi = 0.2$. The pattern on the Poincaré section looks a little like a pearl necklace as shown in Fig. 17. Each pearl is a tiny intersection loop of the complicated torus in the phase space with the Poincaré section, and many of them can be strung into a large virtual loop to compose a necklace.

3.2. Gait performance

Gait performance is studied in this section by varying control parameters in the simulation. Learning the effects of the control parameters on gait performance can be a guide in the practice of our walking method. Energy efficiency and walking speed are two core performance indicators researchers always concern about, because they are closely connected with the applications of bipedal walking robots. The energy efficiency of the gait is evaluated by the specific cost [58], which is defined by the energy cost for a unit weight to walk a unit distance. Walking speed is measured by the Froude number [58]. Because the parameters in our simulation have been non-dimensionalized, the Froude number equals to the ratio of walking distance to time cost.

Observing the gait performance in Figs. 18 and 19, the energy efficiency measured by specific cost is mainly distributed in the interval [0.02, 0.4], and the walking speed measured by the Froude number is mainly distributed in the interval [0.2, 0.45]. In recent studies, Narukawa et al. [21], Hera et al. [24] and Feng et al. [22] reported their results about the level-ground walking of a bipedal robot with a torso. In Narukawa's result, their walking performance is at a roughly equal level with ours; however, when walking at high speed, like 0.4472, the torso leans forward significantly about 0.6 rad [21] throughout the walking process of their gait, while in our result, e.g., in Fig. 7(a), the torso sways around the upright position during walking, which is much more natural. Large torso inclination also occurred in Hera's result [24], in which the leaning angle is between 0.6 and 0.8 rad during walking. Feng et al.'s robot [22] can walk as fast as 0.38 in simulation and the specific cost interval is [0.03, 0.2] for the stable period-1 gait; however, the performance of our gait is better than that. From the speed point of view, our method can realize higher speed; combined with the energy efficiency, our method can generate a more efficient gait, or a faster gait with only 0.2 specific cost.

There is an unstable period-1 gait embedded in the bifurcation gait. It can be seen from the performance figures that the embedded unstable period-1 gait has advantages in terms of walking speed and energy efficiency compared with the bifurcation gait. Generally speaking, the performance of the

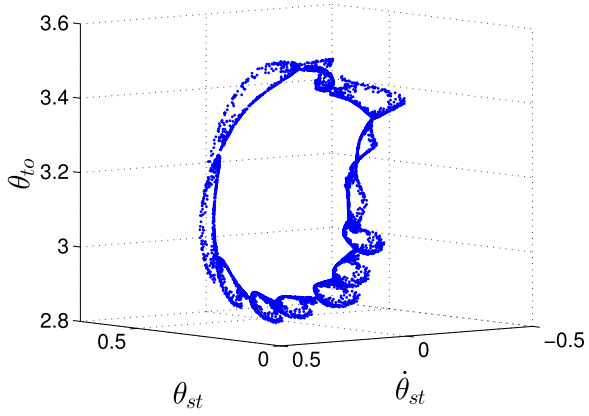

Fig. 17. The projection of the Poincaré section of the Neimark–Sacker-X bifurcation gait ($t_1 = 0.17$, $t_2 = 0.17$, and $\Phi = 0.2$) in the $\theta_{st} - \dot{\theta}_{st} - \theta_{to}$ subspace.

unstable period-1 gait continues the development trend of the stable period-1 gait, yet the performance of the bifurcation gait becomes worse. When Φ is less than 0.2 and t_1 and t_2 are small, the energy efficiency of the bifurcation gait is slightly better than that of the unstable period-1 gait, which is because the average speed of the bifurcation gait is obviously worse than that of the unstable period-1 gait. Therefore, in general, the unstable period-1 gait still has some advantages. When bifurcation occurs, if higher performance is required, control should be introduced to suppress the bifurcation gait and stabilize the embedded unstable period-1 gait; nevertheless, if gait diversity is welcomed, the bifurcation should be sustained without any extra control.

4. Gait bifurcation control

The previous section noted that the embedded unstable period-1 gait has advantages in energy efficiency and walking speed, therefore, in an application emphasizing walking performance, gait bifurcation control with tiny control costs can be used to stabilize unstable period-1 gait instead of bifurcation gait for better performance. The OGY method is a classical chaos control technique, which stabilizes a chaotic attractor to an existing and known time-periodic motion by making only small perturbations of available system parameters [48]. Meanwhile, only employing small parameter perturbations makes this method economical in control cost. According to previous studies [50–52], this method

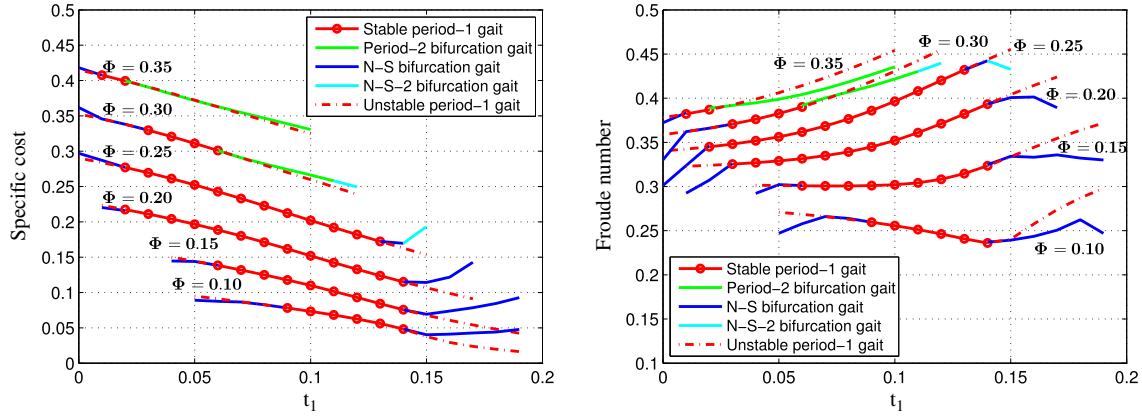

(a) Energy efficiency measured by specific cost.

(b) Walking speed measured by Froude number.

Fig. 18. Gait performance with respect to t_1 for multiple Φ ($t_2 = 0.17$).

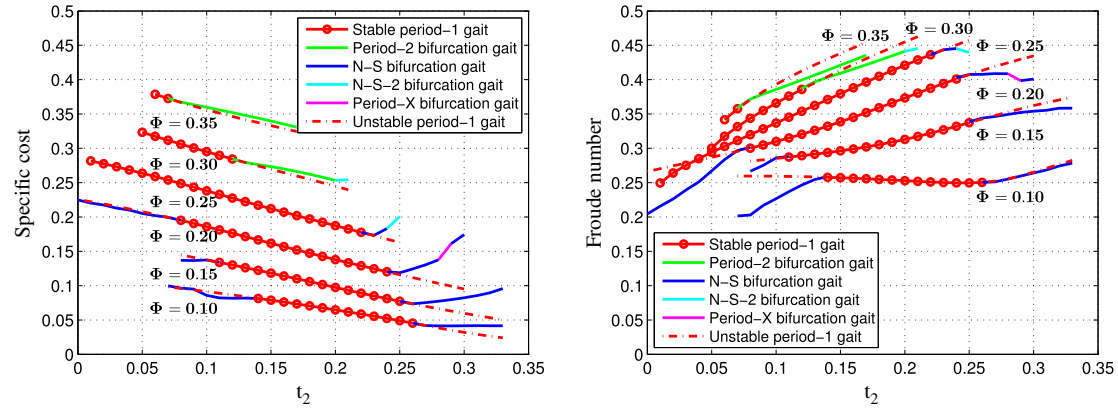

(a) Energy efficiency measured by specific cost.

(b) Walking speed measured by Froude number.

Fig. 19. Gait performance with respect to t_2 for multiple Φ ($t_1 = 0.1$).

is also effective for the period-doubling bifurcation gaits. In this section, the OGY method will be used to suppress the bifurcation gaits in our model, including the Neimark–Sacker bifurcation, and re-generate the period-1 gaits for better performance.

The OGY method is a control method based on the linearization of the Poincaré map, which uses state feedback to assign the pole positions of the closed-loop system. The parameter perturbation is applied in each step to stabilize the unstable period-1 fixed point in its small neighborhood. The concrete operations of the OGY method in gait bifurcation control are as follows. First, the Poincaré map in Section 2.3.3 is expanded to have varying parameters, and this new Poincaré map is denoted as $\boldsymbol{F}'(\boldsymbol{s}, \boldsymbol{p})$, in which $\boldsymbol{p}$ is composed of perturbed parameters of the system. Then, like in Eq. (16), there is $\boldsymbol{s}_{n+1} = \boldsymbol{F}'(\boldsymbol{s}_n, \boldsymbol{p}_n)$ where $\boldsymbol{s}_n$ is the initial state of the nth step, and $\boldsymbol{p}_n$ is the parameters of the nth step. After defining the period-1 fixed point $\boldsymbol{s}^*$ with the nominal parameters $\boldsymbol{p}^*$, we have $\boldsymbol{s}^* = \boldsymbol{F}'(\boldsymbol{s}^*, \boldsymbol{p}^*)$. Linearizing $\boldsymbol{F}'$ of the nth step at its fixed point with the nominal parameters, there is:

$$\boldsymbol{s}_{n+1} - \boldsymbol{s}^* = \boldsymbol{A} \cdot (\boldsymbol{s}_n - \boldsymbol{s}^*) + \boldsymbol{B} \cdot (\boldsymbol{p}_n - \boldsymbol{p}^*) \tag{17}$$

where $\boldsymbol{A} = \frac{\partial \boldsymbol{F}'}{\partial \boldsymbol{s}}(\boldsymbol{s}^*, \boldsymbol{p}^*)$ and $\boldsymbol{B} = \frac{\partial \boldsymbol{F}'}{\partial \boldsymbol{p}}(\boldsymbol{s}^*, \boldsymbol{p}^*)$. Then the control law based on the OGY method, namely the parameter for the nth step, is:

$$\boldsymbol{p}_n = \begin{cases} \boldsymbol{p}^* - \boldsymbol{K} \cdot (\boldsymbol{s}_n - \boldsymbol{s}^*) & \|\boldsymbol{s}_n - \boldsymbol{s}^*\| < \eta_{\boldsymbol{s}} \text{ or } \|\boldsymbol{p}_n - \boldsymbol{p}^*\| < \eta_{\boldsymbol{p}} \\ \boldsymbol{p}^* & \text{other} \end{cases} \tag{18}$$

where $\boldsymbol{K}$ is the gain matrix for feedback, determined by the two Jacobian matrices $\boldsymbol{A}$ and $\boldsymbol{B}$ and the desired closed-loop poles. The basic principle for pole assignment is to make the eigenvalues of $\boldsymbol{A} - \boldsymbol{B} \cdot \boldsymbol{K}$ all locate inside the unit cycle. $\eta_{\boldsymbol{s}}$ is the threshold of the distance between the current state and the fixed point, and $\eta_{\boldsymbol{p}}$ is the threshold of the size of the parameter perturbation. The conditions in Eq. (18) indicate that OGY control is locally active in a limited sphere in phase space or parameter space.

Applying control based on the OGY method (OGY control for short hereafter) to the period-2 bifurcation case ($t_1 = 0.1$, $t_2 = 0.14$, and $\Phi = 0.3$) and the Neimark–Sacker bifurcation case ($t_1 = 0.1$, $t_2 = 0.25$, and $\Phi = 0.2$) in Section 3.1, the two bifurcation gaits are successfully suppressed and converge to the corresponding period-1 gait, as shown in Fig. 20. In our model, actually, all three control parameters can be perturbed. In this case, we select $[t_1, t_2]^T$ to be the perturbed parameter vector $\boldsymbol{p}$. Perturbing two parameters at once is more effective in suppressing bifurcation gait, meanwhile, the identical physical meanings, the serial relationship in actuation process and the similar effects on the gait of t_1 and t_2 make it very easy for the system to be expanded from just perturbing one of them to perturbing both, which make them a good choice. Φ will remain unperturbed in the following examples.

In the above two cases, the eigenvalues of $\boldsymbol{A}$ at the unstable fixed points are $[-1.0107, 0.8284 + 0.4565i, 0.8284 - 0.4565i, 0.4966, -0.0158, 0]^T$ and $[0.8426 + 0.5414i, 0.8426 - 0.5414i, -0.9199, 0.4746, -0.0163, 0]^T$, respectively. Because the

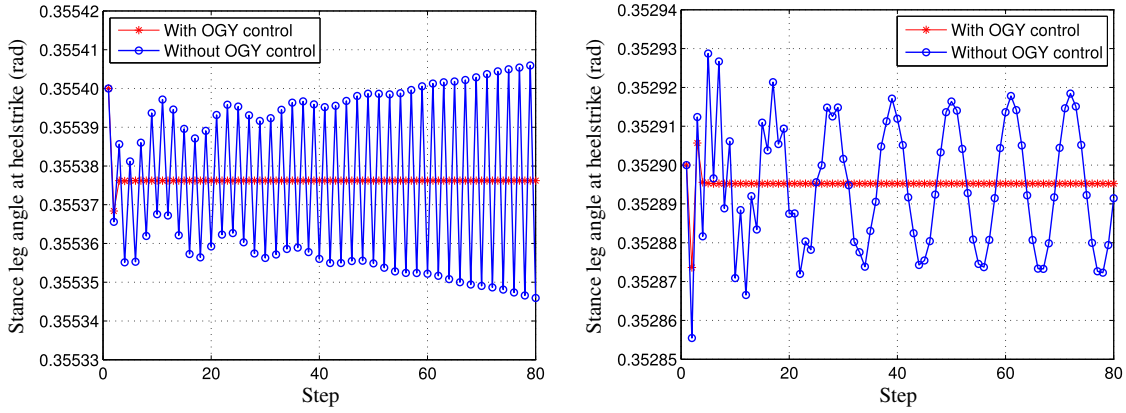

(a) Period-2 bifurcation case. (b) Neimark–Sacker bifurcation case.

Fig. 20. Comparison of the gaits with and without OGY control for two types of gait bifurcations as examples.

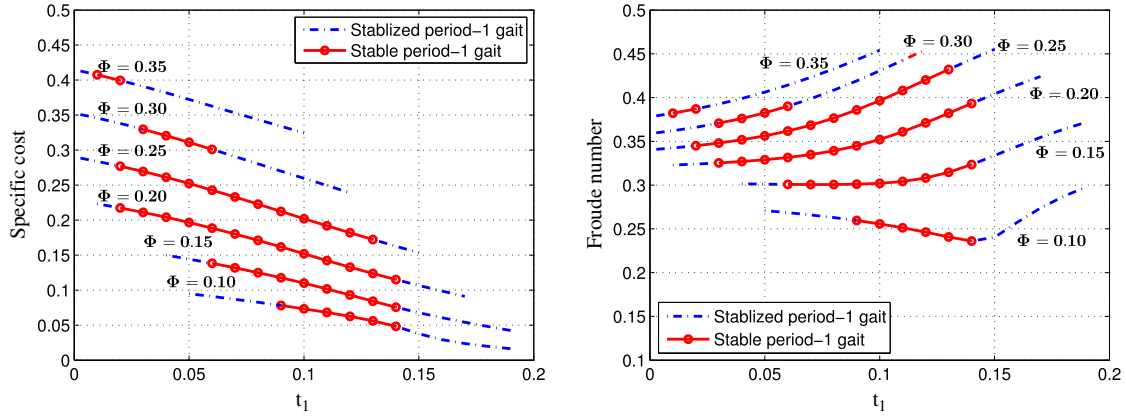

(a) Energy efficiency measured by specific cost. (b) Walking speed measured by Froude number.

Fig. 21. Gait performance of the stabilized gait by OGY control with respect to t_1 for multiple Φ ($t_2 = 0.17$).

poles of the closed-loop Poincaré map can be placed arbitrarily, in these cases, we place them near the origin, specifically $[-0.1, 0.075 + 0.05i, 0.075 - 0.05i, 0.05, -0.01, 0]^T$. Starting from an initial state in the neighborhood of the unstable fixed point, the state on the Poincaré section of the gait with OGY control rapidly converges to the fixed point within five steps, and that without control diverges and finally changes into the corresponding bifurcation pattern.

After applying OGY control, the energy efficiency and the walking speed of the stabilized period-1 gait under $t_1 = 0.1$, $t_2 = 0.14$, and $\Phi = 0.3$ are 0.2743 and 0.4045, respectively, and those of the stabilized period-1 gait under $t_1 = 0.1$, $t_2 = 0.25$, and $\Phi = 0.2$ are 0.1160 and 0.4073, respectively, which are the same as the performance data of the embedded unstable period-1 gait. Meanwhile, the size of the parameter perturbation is less than one ten-thousandth of the corresponding nominal parameter, so the control cost is small and hardly affects the energy efficiency of walking.

Without OGY control, when the walking motion has already diverged to a bifurcation pattern, under $t_1 = 0.1$, $t_2 = 0.14$, and $\Phi = 0.3$, the energy efficiency and the walking speed are 0.2773 and 0.4013, respectively, and those under $t_1 = 0.1$, $t_2 = 0.25$, and $\Phi = 0.2$ are 0.1190 and 0.4055, respectively. Comparing the above data with that of the stabilized period-1 gait, the latter are better, coinciding with the result in Section 3.2.

Fig. 21 shows the gait performance with OGY control with respect to t_1. These results further illustrate that OGY control can deal with various types of bifurcation in our model. The performance data of the stabilized period-1 gait is almost identical to that of the embedded period-1 gait and better than that of the bifurcation gait in Fig. 18, which demonstrates that gait performance can be improved by applying OGY control to the bifurcation gait. Due to space limitations in this paper, the gait performance with OGY control with respect to t_2 is not shown here.

5. Conclusion and discussion

This paper proposed a level-ground walking model based on hip series elastic actuators for a bipedal robot with a torso. Installed between the torso and each leg, the SEAs support the torso while injecting energy into the system to achieve stable walking on level ground. The walking process is controlled by a state machine driven by the events of the landing impact and actuation durations. The actuators in the SEAs actively change the deformations of the elastic elements to couple the energy into the system via elastic potential energy, which transforms the energy provided by the actuators into the kinetic energy of the robot to balance the energy loss at the impact. The actuation only takes place for a short period of time at the beginning of each step and the rest of the step remains passive, producing an efficient and natural gait. In the results of numerical simulations, stable period-1 fixed points were observed, demonstrating the feasibility of the method in generating stable level-ground walking. In addition to the period-1 case, various bifurcation phenomena are discovered. Bifurcation gaits are varied in walking patterns, which is a good illustration of the diversity of the gait; meanwhile, the embedded unstable period-1 gait has advantages in walking performance.

By applying OGY control, the unstable period-1 gait embedded in the bifurcation gait can be stabilized, producing higher energy efficiency and walking speed.

OGY control is based on linearization and requests small perturbations, therefore, it only takes effect in a small neighborhood around the fixed point in phase space or around the nominal parameter in parameter space, as shown in Eq. (18). For an initial state that is far from the fixed point, the parameter perturbation produced by state feedback will exceed the threshold and turn off OGY control. The bifurcation gaits, unlike the chaotic attractor, do not produce ergodicity, which blocks the activation of OGY control. In practice, it is also impossible to always start from a point nearby the fixed point. Consequently, this limitation will, in many cases, cause problems with the execution of our gait bifurcation control.

In the future, study on the dynamics of the model will be undertaken. Meanwhile, aiming at expanding the limitations of OGY control, a new gait bifurcation control method that is also valid for an initial state far away from the fixed point will be studied for practical application.

Acknowledgments

This work is partly supported by the National Natural Science Foundation of China under Grant 61273357. The authors would like to thank the anonymous reviewers for their valuable suggestions that made possible the improvement of this paper.

Appendix A. Supplementary data

Supplementary material related to this article can be found online at http://dx.doi.org/10.1016/j.robot.2016.01.013.

References

[1] T. McGeer, Passive dynamic walking, Int. J. Robot. Res. 9 (2) (1990) 62–82. http://dx.doi.org/10.1177/027836499000900206.
[2] A. Chatterjee, M. Garcia, Small slope implies low speed for McGeer's passive walking machines, Dyn. Stab. Syst. 15 (2) (2000) 139–157.
[3] M.W. Gomes, Collisionless rigid body locomotion models and physically based homotopy methods for finding periodic motions in high degree of freedom models (Ph.D. thesis), Cornell University, 2005.
[4] T. Chyou, G.F. Liddell, M.G. Paulin, An upper-body can improve the stability and efficiency of passive dynamic walking, J. Theoret. Biol. 285 (1) (2011) 126–135. http://dx.doi.org/10.1016/j.jtbi.2011.06.032.
[5] D. Ka, Z. Mingguo, X. Wenli, Passive dynamic walking with torso, in: Mechatronics and Automation (ICMA), 2012 International Conference on, 2012, pp. 273–278.
[6] F. Farshimi, M. Naraghi, A passive-biped model with multiple routes to chaos, Acta Mech. Sin. 27 (2) (2011) 277–284.
[7] M. Günther, H. Ruder, Synthesis of two-dimensional human walking: a test of the lambda-model, Biol. Cybernet. 89 (2003) 89–106. http://dx.doi.org/10.1007/s00422-003-0414-x.
[8] K. Endo, H. Herr, A model of muscle–tendon function in human walking at self-selected speed, IEEE Trans. Neural Syst. Rehabil. Eng. 22 (2) (2014) 352–362.
[9] D. Palmes, H.U. Spiegel, T.O. Schneider, M. Langer, U. Stratmann, T. Budny, A. Probst, Achilles tendon healing: Long-term biomechanical effects of postoperative mobilization and immobilization in a new mouse model, 2002.
[10] J.H. Challis, D.G. Kerwin, Determining individual muscle forces during maximal activity: Model development, parameter determination, and validation, Hum. Mov. Sci. 13 (1) (1994) 29–61. http://dx.doi.org/10.1016/0167-9457(94)90028-0.
[11] G.A. Pratt, M.M. Williamson, Series elastic actuators, in: Intelligent Robots and Systems 95. 'Human Robot Interaction and Cooperative Robots', Proceedings. 1995 IEEE/RSJ International Conference on, Vol. 1, 1995, pp. 399–406.
[12] J. Pratt, G. Pratt, Intuitive control of a planar bipedal walking robot, in: Robotics and Automation, 1998. Proceedings. 1998 IEEE International Conference on, Vol. 3, 1998, pp. 2014–2021.
[13] J.E. Pratt, B. Krupp, V. Ragusila, J. Rebula, T. Koolen, N. van Nieuwenhuizen, C. Shake, T. Craig, J. Taylor, G. Watkins, P. Neuhaus, M. Johnson, S. Shooter, K. Buffinton, F. Canas, J. Carff, W. Howell, The yobotics-ihmc lower body humanoid robot, in: Intelligent Robots and Systems, 2009. IROS 2009. IEEE/RSJ International Conference on, 2009, pp. 410–411.
[14] J.F. Veneman, R. Ekkelenkamp, R. Kruidhof, F. van der Helm, H. van der Kooij, Design of a series elastic- and bowden cable-based actuation system for use as torque-actuator in exoskeleton-type training, in: Rehabilitation Robotics, 2005. ICORR 2005. 9th International Conference on, 2005, pp. 496–499.
[15] M. Hutter, C.D. Remy, M.A. Hoepflinger, R. Siegwart, Efficient and versatile locomotion with highly compliant legs, IEEE/ASME Trans. Mechatronics 18 (2) (2013) 449–458. http://dx.doi.org/10.1109/TMECH.2012.2222430.
[16] D. Paluska, H. Herr, The effect of series elasticity on actuator power and work output: Implications for robotic and prosthetic joint design, Robot. Auton. Syst. 54 (8) (2006) 667–673. http://dx.doi.org/10.1016/j.robot.2006.02.013.
[17] G.W. Howell, J. Baillieul, Simple controllable walking mechanisms which exhibit bifurcations, in: Decision and Control, 1998. Proceedings of the 37th IEEE Conference on, Vol. 3, 1998, pp. 3027–3032.
[18] T. Narukawa, M. Takahashi, K. Yoshida, Biped locomotion on level ground by torso and swing-leg control based on passive-dynamic walking, in: Intelligent Robots and Systems, 2005. (IROS 2005). 2005 IEEE/RSJ International Conference on, 2005, pp. 4009–4014.
[19] T. Narukawa, M. Takahashi, K. Yoshida, Level-ground walk based on passive dynamic walking for a biped robot with torso, in: Robotics and Automation, 2007 IEEE International Conference on, 2007, pp. 3224–3229.
[20] H. Sasaki, M. Yamakita, Efficient walking control of robot with torso based on passive dynamic walking, in: Mechatronics, ICM2007 4th IEEE International Conference on, 2007, pp. 1–5.
[21] T. Narukawa, M. Takahashi, K. Yoshida, Efficient walking with optimization for a planar biped walker with a torso by hip actuators and springs, ROBOTICA 29 (4) (2011) 641–648. http://dx.doi.org/10.1017/S0263574710000354.
[22] S. Feng, S. Al Yahmadi Amur, Z. Sun, Biped walking on level ground with torso using only one actuator, Sci. China Inf. Sci. 56 (11) (2013) 1–9. http://dx.doi.org/10.1007/s11432-013-5009-0.
[23] E.R. Westervelt, J.W. Grizzle, D.E. Koditschek, Hybrid zero dynamics of planar biped walkers, IEEE Trans. Automat. Control 48 (1) (2003) 42–56.
[24] P.X.L.M. La Hera, A.S. Shiriaev, L.B. Freidovich, U. Mettin, S.V. Gusev, Stable walking gaits for a three-link planar biped robot with one actuator, IEEE Trans. Robot. 29 (3) (2013) 589–601.
[25] F. Zajac, J. Winters, Modeling musculoskeletal movement systems: Joint and body segmental dynamics, musculoskeletal actuation, and neuromuscular control, in: J. Winters, S.-Y. Woo (Eds.), Multiple Muscle Systems, Multiple Muscle Systems, Springer, New York, 1990, pp. 121–148.
[26] T.A. McMahon, Muscles, Reflexs and Locomotion, Princeton University Press, 1984.
[27] J.G.G. Jessica Rose, Human Walking, Williams & Wilkins, 1994.
[28] J. Pratt, Exploiting inherent robustness and natural dynamics in the control of bipedal walking robots (Ph.D. thesis), Massachusetts Institute of Technology, 2000.
[29] M. Wisse, Three additions to passive dynamic walking; actuation, an upper body, and 3d stability, in: Humanoid Robots, 2004 4th IEEE/RAS International Conference on, Vol. 1, 2004, pp. 113–132.
[30] M. Wisse, D.G.E. Hobbelen, A.L. Schwab, Adding an upper body to passive dynamic walking robots by means of a bisecting hip mechanism, IEEE Trans. Robot. 23 (1) (2007) 112–123. http://dx.doi.org/10.1109/TRO.2006.886843.
[31] M.H. Raibert, H.B. Brown Jr., Experiments in balance with a 2d one-legged hopping machine, J. Dyn. Syst. Meas. Control 106 (1) (1984) 75–81.
[32] M.H. Raibert, H.B. Brown, M. Chepponis, Experiments in balance with a 3d one-legged hopping machine, Int. J. Robot. Res. 3 (2) (1984) 75–92. http://dx.doi.org/10.1177/027836498400300207.
[33] M.H. Raibert, Legged Robots that Balance, MIT Press, Cambridge, Mass, 1986.
[34] H. Dong, M.G. Zhao, J. Zhang, N.Y. Zhang, Hardware design and gait generation of humanoid soccer robot stepper-3d, Robot. Auton. Syst. 57 (8) (2009) 828–838. http://dx.doi.org/10.1016/j.robot.2009.03.009. humanoid Soccer Robots.
[35] J. Zhang, M. Zhao, H. Dong, Effect of energy feedbacks on virtual slope walking: I. complementary energy feedback (2009 2009).
[36] M. Zhao, Y. Qiu, Event-based control for pneumatic single-legged hopping robot, in: Mechatronics and Automation (ICMA), 2012 International Conference on, 2012, pp. 297–302.
[37] T. McGeer, Stability and Control of Two-dimensional Biped Walking., Tech. Rep. Technical Report CSS-IS TR 88-01, Simon Fraser University, 1988.
[38] S. Collins, A. Ruina, R. Tedrake, M. Wisse, Efficient bipedal robots based on passive-dynamic walkers, SCIENCE 307 (5712) (2005) 1082–1085. http://dx.doi.org/10.1126/science.1107799.
[39] K. Ono, R. Takahashi, T. Shimada, Self-excited walking of a biped mechanism, Int. J. Robot. Res. 20 (12) (2001) 953–966. http://dx.doi.org/10.1177/02783640122068218.
[40] F. Asano, Z.-w. Luo, Z.-w. Luo, Energy-efficient and high-speed dynamic biped locomotion based on principle of parametric excitation, IEEE Trans. Robot. 24 (6) (2008) 1289–1301. http://dx.doi.org/10.1109/TRO.2008.2006234.
[41] H. Dong, M. Zhao, N. Zhang, High-speed and energy-efficient biped locomotion based on virtual slope walking, Auton. Robots 30 (2) (2011) 199–216. http://dx.doi.org/10.1007/s10514-010-9201-4.
[42] A. Goswami, B. Thuilot, B. Espiau, Compass-like Biped Robot-part i: Stability and Bifurcation of Passive Gaits, Tech. Rep, INRIA, 1996.
[43] S. Iqbal, X. Zang, Y. Zhu, J. Zhao, Bifurcations and chaos in passive dynamic walking: A review, Robot. Auton. Syst. 62 (6) (2014) 889–909.
[44] F. Asano, Z.-W. Luo, On efficiency and optimality of asymmetric dynamic bipedal gait, in: Robotics and Automation, 2009. ICRA'09. IEEE International Conference on, 2009, pp. 1972–1977.
[45] F. Asano, Efficiency analysis of 2-period dynamic bipdal gaits, in: Intelligent Robots and Systems, 2009. IROS 2009. IEEE/RSJ International Conference on, 2009, pp. 173–180.

[46] Y. Harata, F. Asano, K. Taji, Y. Uno, Efficient parametric excitation walking with delayed feedback control, in: Intelligent Robots and Systems, 2009. IROS 2009. IEEE/RSJ International Conference on, 2009, pp. 2934–2939.
[47] Y. Harata, F. Asano, K. Taji, Y. Uno, Efficient parametric excitation walking with delayed feedback control, Nonlinear Dynam. 67 (2) (2012) 1327–1335.
[48] E. Ott, C. Grebogi, J.A. Yorke, Controlling chaos, Phys. Rev. Lett. 64 (11) (1990) 1196.
[49] K. Pyragas, Continuous control of chaos by self-controlling feedback, Phys. Lett. A 170 (6) (1992) 421–428. http://dx.doi.org/10.1016/0375-9601(92)90745-8.
[50] S. Suzuki, K. Furuta, S. Hatakeyama, Passive walking towards running, Math. Comput. Model. Dyn. Syst. 11 (4) (2005) 371–395.
[51] H. Gritli, N. Khraief, S. Belghith, Chaos control in passive walking dynamics of a compass-gait model, Commun. Nonlinear Sci. Numer. Simul. 18 (8) (2013) 2048–2065.
[52] H. Gritli, S. Belghith, N. Khraief, Ogy-based control of chaos in semi-passive dynamic walking of a torso-driven biped robot, Nonlinear Dynam. 79 (2) (2015) 1363–1384. http://dx.doi.org/10.1007/s11071-014-1747-9.
[53] M.J. Kurz, N. Stergiou, An artificial neural network that utilizes hip joint actuations to control bifurcations and chaos in a passive dynamic bipedal walking model, Biol. Cybern. 93 (3) (2005) 213–221. http://dx.doi.org/10.1007/s00422-005-0579-6.
[54] M.J. Kurz, K. Markopoulou, N. Stergiou, Attractor divergence as a metric for assessing walking balance, Nonlinear Dynamics Psychol. Life Sci. 14 (2) (2010) 151–164.
[55] A.H. Hansen, D.S. Childress, E.H. Knox, Roll-over shapes of human locomotor systems: effects of walking speed, Clin. Biomech. 19 (4) (2004) 407–414. http://dx.doi.org/10.1016/j.clinbiomech.2003.12.001.
[56] M. Gomes, A. Ruina, Walking model with no energy cost, Phys. Rev. E 83 (3) (2011) 032901. http://dx.doi.org/10.1103/PhysRevE.83.032901.
[57] U.D. Croce, P.O. Riley, J.L. Lelas, D.C. Kerrigan, A refined view of the determinants of gait, Gait & Posture 14 (2) (2001) 79–84. http://dx.doi.org/10.1016/S0966-6362(01)00128-X.
[58] D.G.E. Hobbelen, M. Wisse, Limit cycle walking, in: M. Hackel (Ed.), Humanoid Robots, Human-Like Machines, Humanoid Robots, Human-Like Machines, I-Tech Education and Publishing, 2007.

Ka Deng is a Ph.D. student of Department of Automation, Tsinghua University, Beijing, China. He received his B.E. degree from Xidian University, Xi'an, China, in 2006. His current research interests include biped locomotion, compliance in robot design and active walking method.

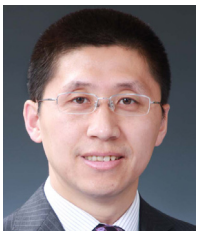

Mingguo Zhao is an Associate Professor of Department of Automation, Tsinghua University. He received his B.E., M.Sc. and Ph.D. degrees from Harbin Institute of Technology in 1995, 1997 and 2001 respectively. From 2001 to 2003, he held a postdoctoral position in Department of Precision Instrument, Tsinghua University. His current research interests include biped locomotion control and robot self-localization.

Wenli Xu is a Professor of Tsinghua University, Beijing China. He received the B.S. degree in Electrical Engineering and the M.E. degree in Automatic Control Engineering from Tsinghua University, Beijing, China, in 1970 and 1980, respectively, the Ph.D degree in Electrical and Computer engineering from the University of Colorado at Boulder, CO, in 1990. His research interests are mainly in the areas of automatic control and computer vision.